Article

Structural Insight into the Mechanism of σ32-Mediated Transcription Initiation of Bacterial RNA Polymerase

Qiang Lu [†], Taiyu Chen [†], Jiening Wang [†], Feng Wang, Wenlong Ye, Lixin Ma *[ID] and Shan Wu *[ID]

State Key Laboratory of Biocatalysis and Enzyme Engineering, Hubei Collaborative Innovation Center for Green Transformation of Bio-Resources, Hubei Key Laboratory of Industrial Biotechnology, School of Life Sciences, Hubei University, Wuhan 430062, China; luqiang@stu.hubu.edu.cn (Q.L.)
* Correspondence: malixing@hubu.edu.cn (L.M.); wushan91@hubu.edu.cn (S.W.)
† These authors contributed equally to this work.

Abstract: Bacterial RNA polymerases (RNAP) form distinct holoenzymes with different σ factors to initiate diverse gene expression programs. In this study, we report a cryo-EM structure at 2.49 Å of RNA polymerase transcription complex containing a temperature-sensitive bacterial σ factor, $σ^{32}$ ($σ^{32}$-RPo). The structure of $σ^{32}$-RPo reveals key interactions essential for the assembly of *E. coli* $σ^{32}$-RNAP holoenzyme and for promoter recognition and unwinding by $σ^{32}$. Specifically, a weak interaction between $σ^{32}$ and −35/−10 spacer is mediated by T128 and K130 in $σ^{32}$. A histidine in $σ^{32}$, rather than a tryptophan in $σ^{70}$, acts as a wedge to separate the base pair at the upstream junction of the transcription bubble, highlighting the differential promoter-melting capability of different residue combinations. Structure superimposition revealed relatively different orientations between βFTH and $σ_4$ from other σ-engaged RNAPs and biochemical data suggest that a biased $σ_4$–βFTH configuration may be adopted to modulate binding affinity to promoter so as to orchestrate the recognition and regulation of different promoters. Collectively, these unique structural features advance our understanding of the mechanism of transcription initiation mediated by different σ factors.

Keywords: Cryo-EM; transcription initiation; RNAP; $σ^{32}$

1. Introduction

Initiation of DNA transcription is one of the main regulatory steps in the control of gene expression. During bacterial transcription initiation, σ factors associate with the RNAP core enzyme, guide the transcription machinery to promoter regions of genes, and engage double-strand promoter DNA [1,2]. The resulting transition from closed RNAP–promoter complex (RPc) to open RNAP–promoter complex (RPo) with melted base pairs (bp) leads to de novo RNA synthesis. Different elements in the promoter DNA, including the −35, extended −10, −10, and discriminator elements, engage intensive interaction with σ factors. Primary σ factor (group 1) is responsible for transcription of housekeeping genes, while alternative σ factors (group 2, group 3, and group 4) control transcription of genes during adaptation to certain intracellular and environmental signals [3,4]. One group of σ factors belonging to the $σ^{54}$ family is involved in nitrogen metabolism and certain stress responses [5,6].

The group 1 factors, represented by $σ^{70}$, are the most studied and well-known factors. *E. coli* $σ^{70}$ is composed of multiple domains, including $σ_{1.1}$, $σ_{1.2}$, $σ_{NCR}$, $σ_2$, $σ_{3.1}$, $σ_{3.2}$ and $σ_4$. $σ_{1.1}$ serves as a gatekeeper, admitting the promoter in and affecting the switching of RNAP properties [7–9]. $Σ_{1.2}$ is responsible for discriminator motif recognition [10]. $Σ_{NCR}$ participates in DNA interaction around the transcription start site [11]. $Σ_{3.1}$ plays a role in "extended −10 motif" recognition and promoter binding [12,13]. $Σ_{3.2}$ threads the RNAP and makes extensive interactions in the active center cleft, thereby affecting primer binding

and promoter escape [14–16]. σ_2 contacts the clamp helices of the β′ subunit and mediates sequence-specific interactions with the promoter −10 element, while σ_4 contacts the β-flap tip helix (βFTH) and mediates sequence-specific interaction with the promoter −35 element [17]. In contrast, group 2 σ factors (such as *E. coli* σ^{38}) lack the σ_{NCR} domain, group 3 σ factors (such as *E. coli* σ^{28} and σ^{32}) lack $\sigma_{1.1}$, σ_{NCR}, and $\sigma_{1.2}$ domains, and group 4 σ factors (such as *E. coli* σ^{24} and σ^{19}) contain only two essential domains: σ_2 and σ_4.

The group 3 σ factor, σ^{32}, plays a pivotal role in the heat shock response (HSR) required by *E. coli* to sustain protein homeostasis and cope with heat and other stresses [18]. σ^{32} synthesis is modulated by the secondary structure of the 5′ region of σ^{32} mRNA, which serves as a "thermometer", responding to temperature changes [19,20]. When the temperature for growing *E. coli* cells suddenly increases, σ^{32} is rapidly synthesized (induction phase) and then directs RNA polymerase to promote transcription of a set of HSR genes to respond to environmental temperature changes [21]. The overproduced σ^{32} is gradually decreased by a set of conserved chaperones (such as DnaK/DnaJ) and proteases that accumulate during the induction phase [22,23].

In *E. coli*, the transcription initiation complex structures of σ^{70} [11,24], σ^{38} [25], σ^{28} [26], σ^{24} [15], and σ^{54} [27–29] have greatly advanced our understanding of how σ factors recognize corresponding promoter elements and initiate transcription. However, the structure of the RNAP holoenzyme or transcription initiation complex that interacts with group 3 σ^{32} or group 4 σ^{19} remains unknown. In this study, we assembled the functional *E. coli* transcribing complex with σ^{32} and determined the structure at 2.49 Å resolution. The structure shows that σ^{32} intensively interacts with promoter −10 and −35 element. Furthermore, several unique structural features were observed and the roles of key amino acids involved were validated through mutagenesis studies.

2. Materials and Methods

2.1. E. coli σ³² or σ³² Derivatives

E. coli strain BL21(DE3) (Novagen, Beijing, China) was transformed with plasmid pET28a-rpoH. Single colonies of the resulting transformants were used to inoculate 50 mL LB broth containing 50 μg/mL Kanamycin and cultures were incubated, with shaking, for 16 h at 37 °C. Aliquots (10 mL) were used to inoculate 1 L LB broth containing 50 μg/mL Kanamycin and cultures were incubated, with shaking, at 37 °C until OD_{600} = 0.6. The cultures were induced by adding IPTG to 1 mM and incubated for 3 h at 37 °C. Then, the cells were harvested by centrifugation (5000 rpm for 10 min at 4 °C), resuspended in 20 mL buffer A (20 mM Tris–HCl, pH 8.0; 0.1 M NaCl; 1.5% glycerol) and lysed using a JN-02C cell disrupter (JNBIO, Guangzhou, China). The lysate was centrifuged (12,000 rpm for 45 min at 4 °C) and the supernatant loaded onto a 2 mL column of Ni-NTA agarose (Qiagen, Wuhan, China) equilibrated with buffer A. The column was washed with 10 mL buffer A containing 0.16 M imidazole and eluted with 10 mL buffer A containing 0.5 M imidazole. The sample was further purified using a 5 mL column of HiTrap Heparin HP (GE Healthcare, Boston, MA, USA) equilibrated in buffer A and eluted using a 100 mL linear gradient of 0.2–1 M NaCl in buffer A. Fractions containing *E. coli* σ^{32} or σ^{32} derivatives were pooled and stored at −80 °C.

2.2. E. coli RNAP Core Enzyme

E. coli RNAP core enzyme was prepared from *E. coli* strain BL21(DE3) (Invitrogen, Inc., Carlsbad, CA, USA) transformed with plasmid pET28a-rpoA-rpoB-rpoC-rpoZ similar to pIA900 [30]. Single colonies of the resulting transformants were used to inoculate 50 mL LB broth containing 50 μg/mL Kanamycin, and cultures were incubated, with shaking, for 16 h at 37 °C. Aliquots (10 mL) were used to inoculate 1 L LB broth containing 50 μg/mL Kanamycin, cultures were incubated at 37 °C, with shaking, until OD_{600} = 0.6 and then induced by adding IPTG to 1 mM. The cultures were incubated for 3 h at 37 °C. The cells were subsequently harvested by centrifugation (5000× *g* for 10 min at 4 °C), resuspended in 20 mL lysis buffer (50 mM Tris-HCl, pH 7.9; 0.2 M NaCl; 2 mM EDTA; 5% glycerol; and

5 mM DTT), and then lysed using a JN-02C cell disrupter. After poly-ethyleneimine precipitation and ammonium sulfate precipitation, the pellet was resuspended in buffer B (10 mM Tris-HCl, pH 7.9; 0.5 M NaCl; and 5% glycerol) and loaded onto a 5 mL column of Ni-NTA agarose equilibrated with buffer B. The column was washed with 25 mL buffer B containing 20 mM imidazole and eluted with 25 mL buffer B containing 0.15 M imidazole. The eluate was diluted in buffer C (10 mM Tris-HCl, pH 7.9; 0.2 M NaCl; and 5% glycerol) and loaded onto a Mono Q 5/10 GL column (GE Healthcare, Boston, MA, USA) equilibrated in buffer C and eluted using a 30 mL linear gradient of 0.3–0.5 M NaCl in buffer C. Fractions containing *E. coli* RNAP core enzyme were pooled and stored at −80 °C.

2.3. Nucleic Acid Scaffolds and E. coli σ³²-RPo Assembly

Nucleic acid scaffolds of the σ^{32} consensus promoter dnaKp1 for cryo-EM study of *E. coli* σ^{32}-RPo and for fluorescence polarization study were prepared from synthetic oligos (F: 5′-CCCCCTTGAAGACGTGGTTTACGACCCCATTTAGTAGTCAACCGCAGTGAGTGA-3′; R: 5′-TCACTCACTGCGGTTGACTACTAAATGGGGTCGTAAACCACGTCTTCAAGGGGG-3′) [31] using an annealing procedure (95 °C for 5 min followed by 2 °C step cooling to 25 °C) in annealing buffer (5 mM Tris-HCl, pH 8.0; 200 mM NaCl; and 10 mM MgCl$_2$).

E. coli σ^{32}-RPo, the *E. coli* RNAP core enzyme, *E. coli* σ^{32}, and nucleic acid scaffolds were mixed at 1:4:1.2 molar ratios and incubated at 4 °C overnight. The RPo complexes were purified using a Hiload 16/60 Superdex 200 column (GE Healthcare, Boston, MA, USA) and stored in 20 mM Tris–HCl pH 8.0, 0.1 M NaCl, 1% glycerol, and 1 mM DTT with a concentration of 5 mg/mL.

2.4. In Vitro Transcription Assay

In vitro Mango-based transcription assays [32] were carried out by incubating the *E. coli* RNAP core enzyme, *E. coli* σ^{32} or σ^{32} derivatives, and dnaKp1-mango scaffold. Transcription assays were performed using a 96-well microplate format. Reaction mixtures (40 μL) contained 0.1 μM *E. coli* RNAP holoenzyme, 0.1 μM *E. coli* σ^{32} or σ^{32} derivatives, 50 nM dnaKp1-mango scaffold, 1 μM TO1-Biotin, 0.1 mM NTP mix (ATP, UTP, GTP and CTP), 40 mM Tris–HCl, pH 8.0, 50 mM NaCl, and 10 mM MgCl$_2$. First, the *E. coli* RNAP core enzyme, *E. coli* σ^{32} or σ^{32} derivatives, and dnaKp1-mango scaffold were incubated for 10 min at 37 °C. Following incubation with NTP mix and TO1-biotin for another 10 min at 37 °C, fluorescence emission intensities were measured using a multimode plate reader (EnVision, PerkinElmer Inc.; excitation wavelength = 510 nm; emission wavelength = 535 nm). Relative transcription activities of σ^{32} derivatives were calculated as described in a previous report [32].

2.5. Fluorescence Polarization Assay

We measured the affinity of two FAM-labeled holoenzyme DNA molecules. The shorter DNA (containing the −35 element) was used to validate the role of DNA-contacted amino acids in σ_4 (Figures 1E and 2B), while the longer DNA (containing the sequence from the −35 element to the −10 bubble) was used to validate the effect of σ_4–βFTH configuration changes on affinity (Figure 3F). The sequence of the shorter 6-FAM-labeled DNA template strand was 5′-CCTTGAAGACGTGG-3′ and the nontemplate strand was 5′-CCACGTCTTCAAGG-3′; the sequence of the longer 6-FAM-labeled DNA template strand was 5′-CCTTGAAGACGTGGTTTACGACCCCATTTAGTAG-3′ and the nontemplate strand was 5′-GGGGTCGTAAACCACGTCTTCAAGG-3′. The labeled template strand and the nontemplate strand were annealed in a 1:1 ratio in 10 mM Tris-HCl, pH 7.9 and 0.2 M NaCl and stored at −80 °C. The annealed DNA (5 nM) was incubated with *E. coli* σ^{32} or σ^{32} derivatives holoenzyme (10, 20, 40, 80, 160, and 320 nM) in 100 μL FP-A buffer (10 mM Tris-HCl, pH 7.7; 100 mM NaCl; 1 mM DTT; 1% glycerol; and 0.025% Tween-20) in a 96-well plate (Corning, NYC, USA) for 5 min at room temperature. The fluorescence polarization (FP) signals were measured using a plate reader (SPARK, TECAN, Switzerland)

at excitation wavelength = 494 nm and emission wavelength = 518 nm. The calculated Kd is an apparent Kd obtained from the best-fit curve by fitting our plots to a nonlinear regression equation [33,34].
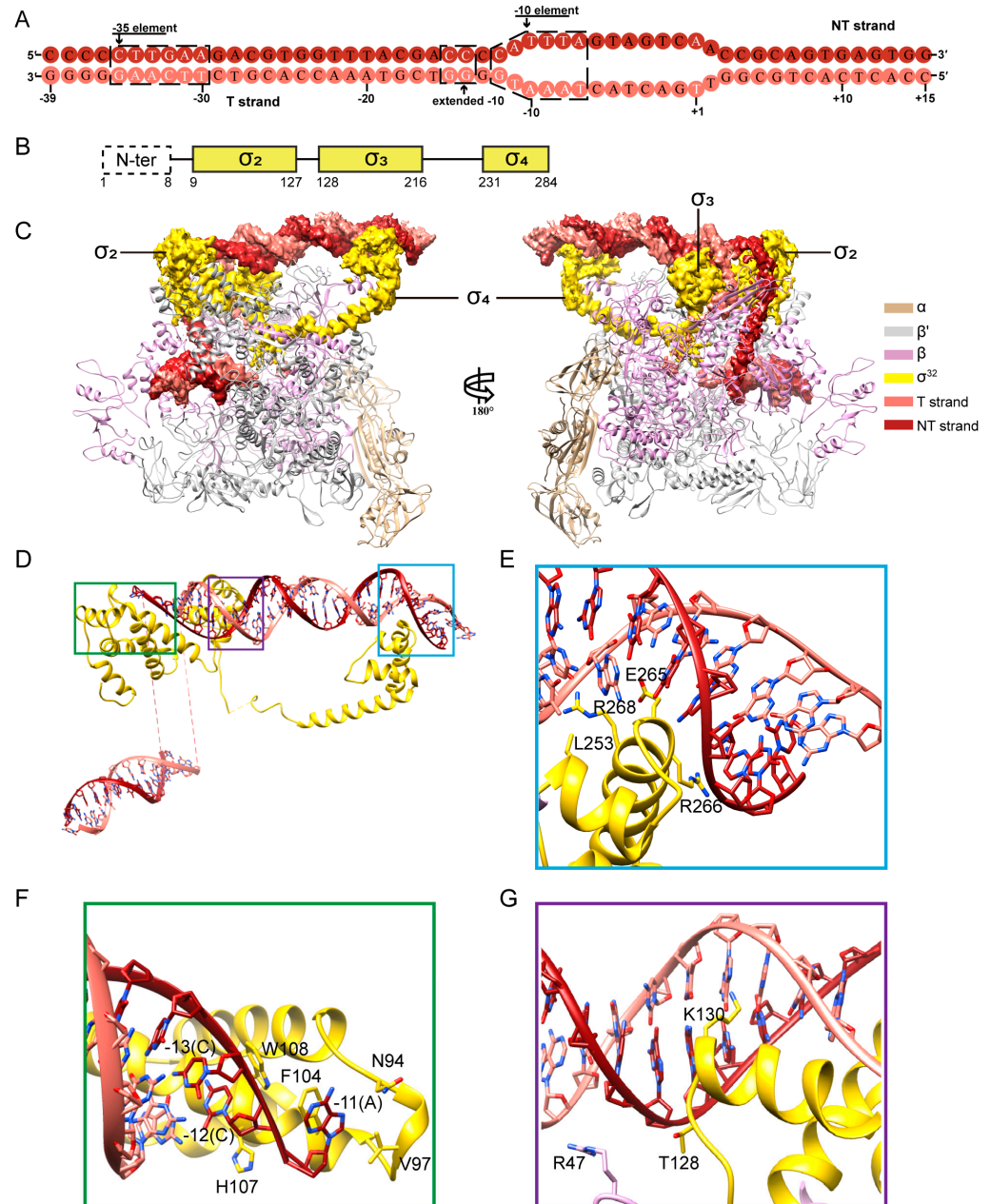

Figure 1. Cryo-EM structure of the *E. coli* σ^{32}-RPo complex and interaction between σ^{32} and promoter DNA. (**A**) Nucleic acid scaffold. A schematic representation of the synthetic promoter DNA scaffold (54-bp) in the σ^{32}-RPo. The −35, −10, and the extended −10 elements are annotated by a dashed box. Positions are numbered relative to the transcription start site. (**B**) Domain architecture of σ^{32}, N-ter fragment of σ^{32} in the empty frame was not modeled in our structure. (**C**) Overviews of the structure and partial cryo-EM reconstruction maps of the *E. coli* σ^{32}-RPo. The subunits of β', β, α, T strand, NT strand, and σ^{32} are colored light brown, purple, gray, yellow, hot pink, and maroon, respectively. The individual domain of σ^{32} is labeled. (**D**) Overall interaction between σ^{32} and promoter DNA. The dashed boxes indicate the interaction regions. (**E**) Detailed interaction between σ_4 and −35 element of promoter DNA. (**F**) Detailed interaction between σ_2 and −10 element of promoter DNA. (**G**) Detailed interaction between σ_3 and −35/−10 spacer region of promoter DNA.
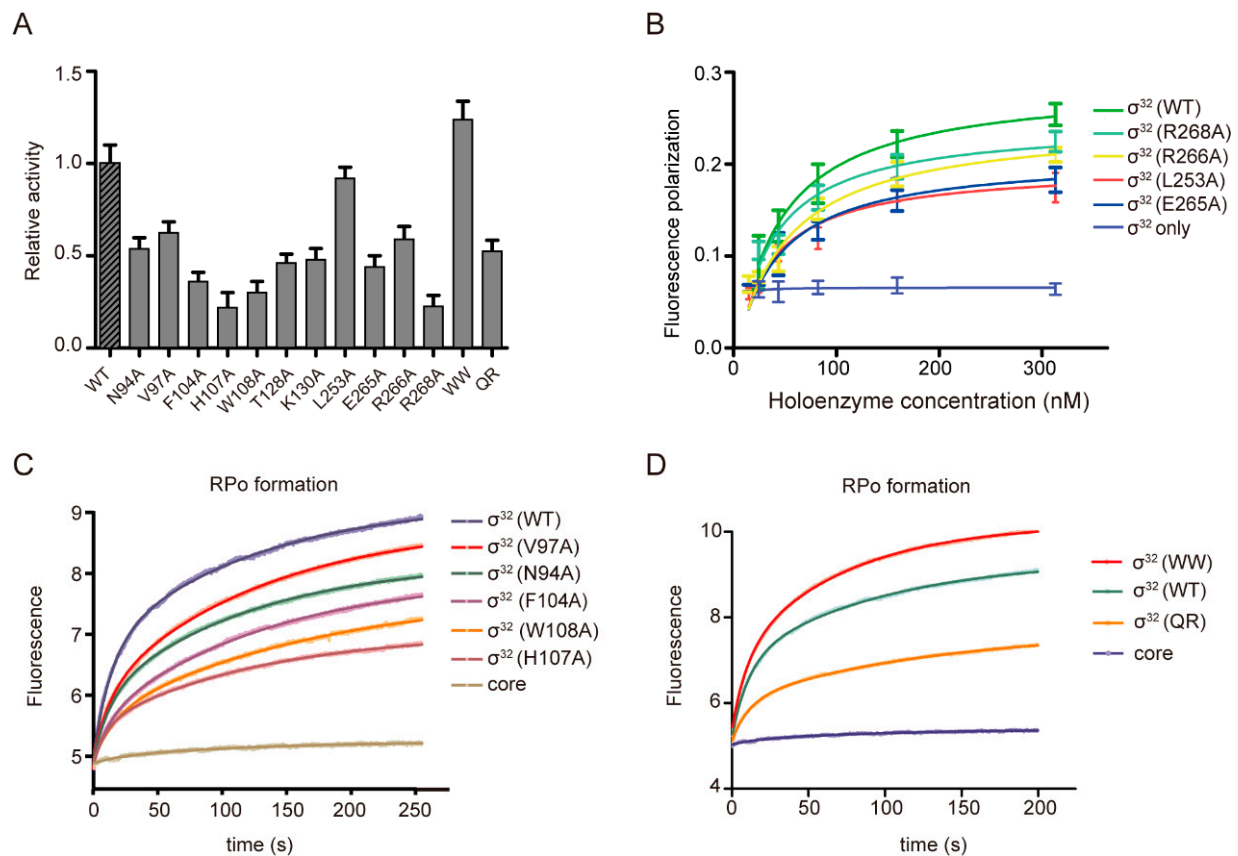
Figure 2. In vitro transcription activity, DNA binding affinity, and promoter unwinding activity of σ^{32} and σ^{32} derivatives. (**A**) In vitro transcription activity of σ^{32} and σ^{32} derivatives. The experiments were conducted in triplicate (mean± SEM; 3 determinations). Error bars represent mean± SEM of n = 3 experiments. (**B**) Binding affinities of wild-type (WT) σ^{32} or σ^{32} derivatives holoenzyme and promoter −35 element measured using fluorescence polarization (FP) assay. (**C**) Promoter unwinding activity of wild-type (WT) σ^{32} or σ^{32} derivatives holoenzyme (σ^{32} derivatives in the "A-11" pocket) measured using stopped-flow assay. (**D**) Promoter unwinding activity of σ^{WW}, σ^{HW} (WT), and σ^{QR} measured using stopped-flow assay.

Fluorescence polarization was calculated using the formula:

$$P = (I_{VV} - I_{VH})/(I_{VV} + I_{VH})$$

where I_{VV} and I_{VH} are fluorescence intensities with the excitation polarizer at the vertical position and the emission polarizer at the vertical position and the horizontal position, respectively. The equilibrium dissociation constant, Kd, was calculated using the equation:

$$P = P_f + \{(P_b - P_f) \times [T]/(Kd + [T])\}$$

where P is the fluorescence polarization at a given concentration of holoenzyme, P_f is the fluorescence polarization of free 6-FAM-labeled promoter DNA, P_b is the fluorescence polarization of bound 6-FAM-labeled promoter DNA, and [T] is the concentration of holoenzyme harboring WT or mutant σ^{32}.
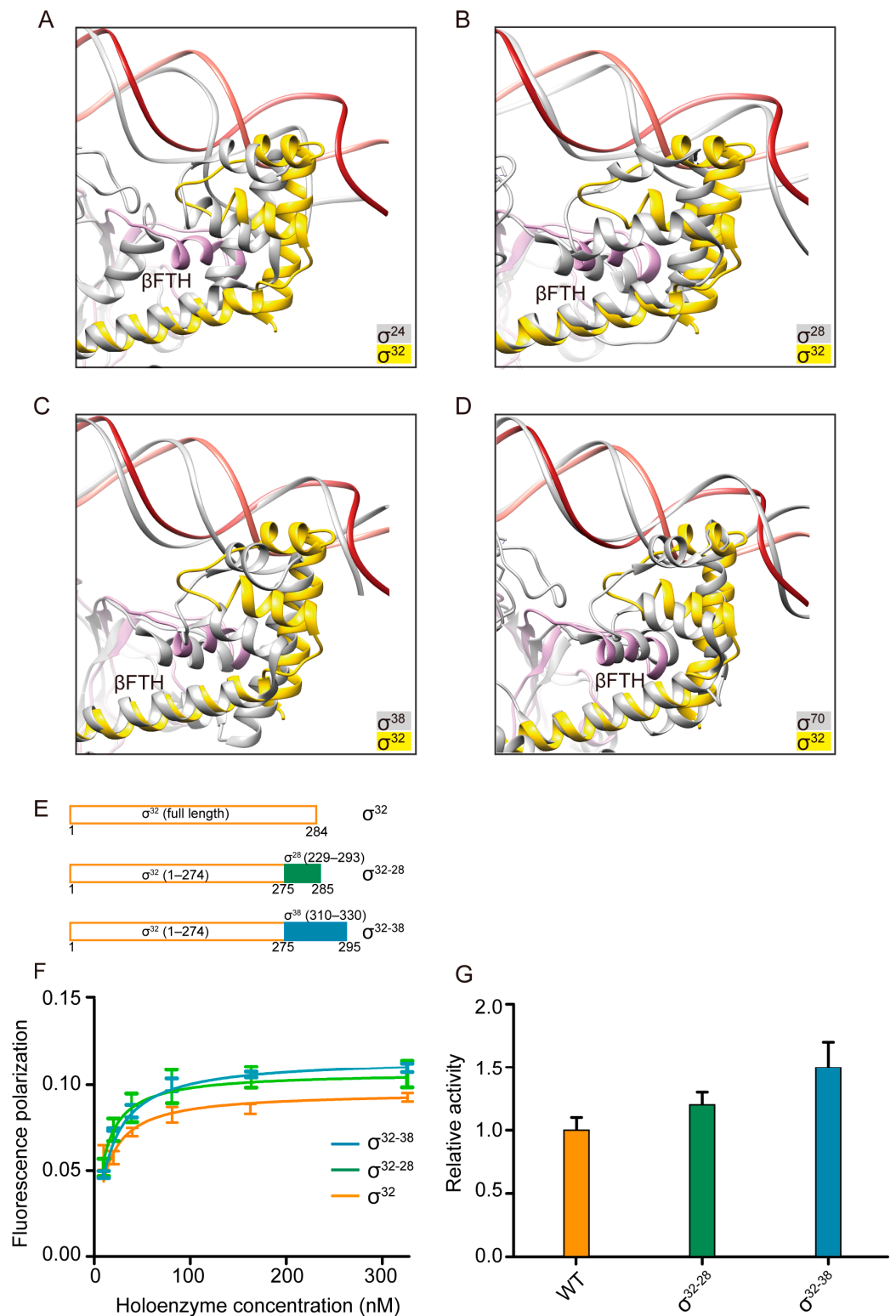
Figure 3. Superimposition and characteristics of βFTH–σ_4 interactions. (**A–D**) Superimposition of βFTH–σ_4 interactions between σ^{32} and σ^{24} (PDB: 6JBQ), σ^{28} (PDB: 6PMI), σ^{38} (PDB: 6OMF), and σ^{70} (PDB: 6CAO), respectively. (**E**) Schematic diagram of the WT, chimera σ^{32-28}, and chimera σ^{32-38}. (**F**) Binding affinities of wild-type σ^{32} or σ^{32} derivative holoenzyme and promoter measured using the FP assay. (**G**) In vitro transcription activities of WT, chimera σ^{32-28}, and chimera σ^{32-38} (mean ± SEM; 3 determinations). Error bars represent mean ± SEM of n = 3 experiments.

2.6. Stopped-Flow Assay

The promoter for the stop flow assay was prepared as previously reported [15]. The Cy3-amido-dT-modified nontemplate-strand primer (*dnaKp1*-Cy3-nontemplate: 5′-GCATCTCCCCCTTGAAGACGTGGTTTACGACCCCATTTAGTAGTC/iCy3dT/ACCGCAGT-3′; 10 μM, Sangon Biotech) and the template-strand primer (*dnaKp1*-template: 5′-GGCACGTACGAATATACCACATACCAATCCTTCCTTCGTACGTGCACTCACTCACTGCGGTTGACTACTAAAT-3′; 10 μM, Sangon Biotech) were processed as previously reported [15]. To monitor the efficiency of RPo formation of *E. coli* RNAP holoenzymes comprising wild-type or derivatives of *E. coli* σ^{32}, 60 μL σ^{32}-RNAP holoenzyme (200 nM) and 60 μL Cy3- PdnaKp1 (4 nM) in 10 mM Tris–HCl (pH 7.7), 20 mM NaCl, 10 mM MgCl$_2$, and 1 mM DTT were rapidly mixed and the change in Cy3 fluorescence was monitored in real time using a stopped-flow instrument (SX20, Applied Photophysics Ltd., UK) equipped with an excitation filter (515/9.3 nm) and a long-pass emission filter (570 nm). The data were plotted in SigmaPlot (Systat software, San Jose, CA, USA) and fitted to eqn: $F = F_0 + a_1 \times (1 - \exp \times (-k_{obs,1} \times t)) + a_2 \times (1 - \exp \times (-k_{obs,2} \times t))$. The amplitudes ($a_1$ and a_2) and observed rates ($k_{obs,1}$ and $k_{obs,2}$) were estimated as previously reported [15,35].

2.7. Cryo-EM Grid Preparation

Grids (Quantifoil 1.2/1.3 Au 300 mesh) were glow-discharged for 25 s at 15 mA prior to application of 4 μL complex at a concentration of 1.2 mg/mL, then plunge-frozen in liquid ethane using a Vitrobot (FEI, Valley, SD, USA.) with 100% chamber humidity at 4 °C.

2.8. Cryo-EM Data Acquisition and Processing

Grids were transferred to a 300 kV Titan Krios electron microscope equipped with a Gatan K3 summit direct electron detector and a GIF energy filter with a slit width of 20 eV. All the images were auto-collected via EPU [36] with a magnification of 105 k and exposure time of 2.5 s using a 0.851 Å pixel size and a defocus ranging from −1.0 to−1.5 μm. The total dose was about 54 e/Å^2. A total of 8555 movies were imported and processed using Relion. All 40 frames were aligned using MotionCor2 [37] before contrast transfer function (CTF) estimations. The contrast transfer function was estimated for each summed image using CTFFIND4 [38]. From the summed images, ~4,000,000 particles were auto-picked and subjected to 2D classification in RELION [39]. 2D averages of the best classes were used as templates for auto-picking in RELION. Auto-picked particles were manually inspected and then subjected to 2D classification in RELION. Poorly populated classes were removed, resulting in a dataset of 641,734 particles. These particles were re-extracted without binning and processed further using 3D refinement and CTF refinement. The final density map was post-processed in RELION with a resolution of 2.49 Å. Focus refinement with mask and signal subtract improved local resolution of the DNA-σ^{32} interaction area to 3.40 Å.

2.9. Cryo-EM Model Building and Refinement

The coordinates of core RNAP and promoter DNA from the structure of *E. coli* core RNAP (PDB: 7MKP) [40] were fitted into the cryo-EM density map using chimera [41] and manually modified in COOT [42]. The coordinates of σ^{32} were manually built in COOT [42]. The coordinates were real-space refined with secondary structure restraints in Phenix [43]. Due to the weak map signal, the region between the −10 bubble and downstream double-stranded DNA was not modeled. The portions of chains C (residues 233–332 and 974–1025) and F (residues 960–1126), which are in low-resolution maps and not the main focus of our work, were also not modeled.

3. Results

3.1. The Cryo-EM Structure of E. coli σ^{32}-RPo

To determine the structure of *E. coli* σ^{32}-RPo, we reconstituted the complex with the *E. coli* RNAP core enzyme, σ^{32}, and a nucleic acid scaffold (Figure 1). The nucleic acid scaffold (−39 to +15; +1 as transcription start site) is composed of a 28-bp upstream

double-stranded DNA (dsDNA) with consensus sequences of the -35 element, a 13-bp transcription bubble (complementary sequences on both strands), and a 13-bp downstream dsDNA (Figure 1A).

We obtained a cryo-EM map at 3.0 Å for the *E. coli* σ^{32}-RPo complex with local resolution at the active-center cleft of RNAP around 2.49 Å (Figure 1C and S1 and Table 1). The map shows clear densities for residues of σ_2 (residues 47–127) and σ_4 (residues 231–279) (Figure 1B,C). The map also shows clear densities for the upstream part of the transcription bubble and the downstream dsDNA (Figure 1C,D). Similar to studies on other σ factors [11,44], the overall structure of RNAP shows minimal structural change upon σ^{32} engagement. Structural superimposition between RNAP core (PDB 7MKP) and σ^{32}-RNAP results in an RMSD of 1.633 Å across 3268 residues [45]. Similar to other σ factors, the RNAP clamp in the structure of σ^{32}-RPo remains in a closed conformation (Figure 1C). The omega subunit is absent from the solved structure, probably due to low binding affinity.

Table 1. Statistics of cryo-EM data and structure refinement.

Data Collection and Processing	RPo
Magnification	105,000
Voltage (kV)	300
Electron exposure (e^-/Å^2)	54
Defocus range (μm)	$-1.0\sim-1.5$
Pixel size (Å)	0.851
Symmetry Imposed	C1
Number of micrographs	8557
Initial particle projections (no.)	3,854,813
Final particle projections (no.)	641,734
Map resolution (Å)	2.49
FSC threshold	0.143
Map resolution range	2.3–7.0
Refinement	
Initial model used	PDB 7MKP
Model resolution (Å)	2.64
FSC threshold	0.143
Map sharpening B factor (Å^2)	-10
Model composition	
Nonhydrogen atoms	28,255
Protein residues	3386
Nucleotides	83
B factors (Å^2)	
Protein	8.12/205.39/64.84
Nucleic acids	94.01/275.47/208.74
Validation	
MolProbity score	1.54
Clashscore	6.05
Poor rotamers (%)	0.03
Ramachandran plot	0.00
Favored (%)	96.67
Allowed (%)	3.33
Model to Map	
Map CC	0.8358

In the structure of σ^{32}-RPo, the σ_2 and σ_4 domains bind to the surface of RNAP (Figure 1C). The σ_2 domain attaches to the clamp helices of the β′ subunit of RNAP via a polar surface. The interface residues include D77, E81, I84, and M87 of σ^{32}, and R275, R278, R281, L282, L285, I291, E295, and M298 of clamp helix of the β′ subunit (Figure S3A). The σ_4 domain of σ^{32} uses a distinct hydrophobic surface to bind the βFTH of RNAP. The interface residues include A221, L225, W244, L245, L278 and E283 of the σ_4 domain and E898, K900, L901, I905 and F906 of the βFTH (Figure S3B). Furthermore, σ^{32} strongly interacts with

different DNA elements in the promoter DNA (Figure 1D–G). The N-terminus of σ^{32} was not modeled in the structure, possibly due to the flexibility caused by the presence of intrinsically disordered regions.

3.2. The Interactions between σ_4 Domain and the −35 Element

σ^{32}-regulated promoters have a distinct consensus sequence at their −35 elements (5′-CTTGAA-3′; from −35 to −30). In the structure, σ_4 adopts a helix-turn-helix fold (Figure 1D), inserts into the major groove of dsDNA around the −35 element, and potentially makes base-specific polar interactions with nucleotides (Figure 1E). The interactions are important, as substituting E265, R266, or R268 with alanine resulted in substantial loss of transcription activity (Figure 2A). The effect of L253A is modest compared with that of other residues. Furthermore, the fluorescence polarization assay shows that the substitution of these residues with alanine profoundly decreases binding affinity between σ^{32} and −35 element. The calculated K_D values of L253A, E265A, R266A, and R268A mutants are 38.75 nM, 45.88 nM, 54.87 nM, and 46.72 nM, respectively, while the K_D value of the wild-type σ factor is 28.41 nM, justifying the functional importance of these interactions (Figure 2B). It is worth noting that while σ^{32}-RNAP holoenzyme readily interacts with promoter −35 element DNA, the sole σ^{32} fails to bind DNA (Figure 2B), which is consistent with previous reports that sole σ subunits adopt a closed conformation and are incapable of binding DNA [46,47].

3.3. The Interactions between σ^{32} and −35/−10 Spacer

The interactions between σ factors and −35/−10 spacer were established to stabilize the conformation of the upstream DNA duplex, promoting the engagement of the upstream duplex with σ_4 and σ_2 for subsequent promoter unwinding. The σ^{32}-RPo complex contacts the phosphate backbones of the spacer region between the −35 and the −10 elements at three positions (Figure 1D). Beside the reported interaction between R47 of the RNAP-β′ zipper domain and phosphate backbones of nucleotides between $G_{−17}$ and $C_{−18}$ on the nontemplate DNA strand, σ^{32} was also found to interact with −35/−10 spacer. Specifically, T128 contacts the same phosphate backbones of nucleotides between $G_{−17}$ and $C_{−18}$. K130 of σ^{32} makes a H-bond with N7 atoms of $G_{−15}$ on the template DNA strand, which together with $G_{−14}$ were identified to be the "extend −10" element [48] (Figure 1G). Substituting T128 and K130 with alanine causes a substantial loss of transcription activity (Figure 2A), highlighting the importance of these interactions [48].

3.4. The Promoter-DNA-Unwinding Function of σ^{32}

σ^{70}, σ^{38}, and σ^{28} of *E. coli* unwind promoter DNA at the −11/−12 junction [26,44,49], while σ^{24} unwinds promoter DNA at a position 1 bp upstream of the transcription bubble [15]. Our structure shows that the C:G bases at position −12 are paired, while the A:T bases at position −11 are unwound (Figure 1F). This observation strongly suggests that σ_2 unwinds promoter DNA at the −11/−12 junction, which is consistent with that of σ^{70} [49,50]. Specifically, H107 blocks the path upstream dsDNA and serves as a wedge to disrupt base stacking between positions $A_{−11}$ and $C_{−12}$ (Figure 1F). The unwound nucleotide $A_{−11}$ on the nontemplate DNA strand is stabilized by a pocket created by N94, V97, F104, and W108 on the "specificity loop" of σ_2 domain [51] (Figure 1F). A similar pocket is reported where different bases are recognized [11,15]. The functional importance of these residues in transcription was validated by our experiment, which showed that substitution with alanine resulted in significant loss of transcription activity (Figure 2A).

To explore the contributions of these residues in promoter unwinding, we modified a stopped-flow assay to monitor RPo formation by *E. coli* σ^{32}-RNAP, in which the fluorescence of a Cy3 fluorophore at +1 position on the nontemplate DNA strand increases upon RPo formation. As shown in Figure 2C and Table S1, the kinetics of RPo equilibration of σ^{32} (H107A)-RNAP holoenzyme is significantly slower than that of wild-type σ^{32}-RNAP. Mutations in the protein pockets of $A_{−11}$ (N94A, V97A, W108A and F104A) also exhibited

slowed RPo equilibration. It is worth noting that the curves could well fit to a double exponential where the amplitudes and observed rates for the fast (a_1, $k_{obs,1}$) and slow (a_2, $k_{obs,2}$) phases were fixed [35] (Table S1), suggesting the existence of a significant intermediate (RPi) on the path to RPo formation. The amplitudes (a_1, a_2) describe that phase's contribution to the total fluorescent enhancement signal. As show in Table S1, the amplitude of the curve is dominated by the amplitude of the slow rate, which implies that the slow phase contributes more to final RPo formation. As fluorescence enhancement serves as a reporter of the open complex, we conclude that substituting these residues with alanine significantly destabilizes the open *E. coli* RNAP complex. Specifically, our results show that substituting W108, H107, and F104 with alanine greatly destabilizes the RPo, while substituting V97 and N94 with alanine only slightly destabilizes the RPo (Table S1).

Sequence alignment and structural analysis of other *E. coli* σ factors indicate that diverse residues lie in the same position in different σ factors and play the same role as H107–W108 of σ^{32} (Figures S2 and S4I–L). To compare the efficiency of these residues at promoter unwinding, we substituted the HW residues with WW (σ^{70} and σ^{38}) and QR (σ^{28}), and tested the corresponding transcription activity using a Mango-dependent in vitro transcription assay. As shown in Figure 2A, the rankings in transcription activity differ as follows: $\sigma^{WW} > \sigma^{HW}$ (WT) $> \sigma^{QR}$. Similarly, the RPo formation activity was ranked as $\sigma^{WW} > \sigma^{HW}$ (WT) $> \sigma^{QR}$ (Figure 2D, Table S2), indicating that distinct wedge residues were employed by different σ factors to orchestrate the recognition and unwinding of different promoters. We speculate that the HW motif in σ^{32} evolved from the WW motif in σ^{70} with the purpose of facilitating selective expression of different genes to adapt to changes in internal and external environments. One possibility is that the WH motif, beside its role in helping promoter DNA melting, and together with adjacent residues, may provide a unique structural feature that allows σ^{32} to interact with specific promoters and regulate the expression of heat shock genes.

Notably, the curves and parameters ($k_{obs,1} \sim 0.1^{\mathrm{s}-1}$, $k_{obs,2} \sim 0.01^{\mathrm{s}-1}$) in Figure 2C,D are similar and resemble those in *E. coli* σ^{24}-RNAP [15] rather than those in *M. tuberculosis* CarD-RNAP [52], which means that the observed fast rates ($k_{obs,1} \sim 1^{\mathrm{s}-1}$) report on protein–DNA interaction is not related to opening (i.e., binding) and the observed slow rate ($k_{obs,2} \sim 0.1^{\mathrm{s}-1}$) is related to RPo equilibration. These results indicated the importance of RPo formation for transcription, and also highlighted the multiplicity of RPo equilibration in different bacteria.

3.5. βFTH Adopts a Distinct Conformation to Orchestrate σ^{32}-Promoter Recognition

To date, structures of four σ factors that belong to the σ^{70} family have been resolved, including σ^{70} [11,50], σ^{38} [25,44], σ^{28} [26], and σ^{24} [15]. We compared these published structures to dissect more details about the mechanism of promoter recognition. Structure superimposition revealed that the relative orientation between βFTH and σ_4 in σ^{32}-engaged RNAP differ between these σ-engaged RNAPs (Figure 3A–D). To further explore the role of βFTH in σ-mediated DNA engagement, we designed two chimeric σ factors to validate DNA binding affinity to the corresponding holoenzymes. Considering that (1) σ^{38} recognizes promoters overlap with σ^{70} but σ^{70} is larger than the other σ factors; (2) σ^{28} and σ^{38} belong to the same group 3 category; and (3) the tail of σ^{24} did not observably interact with βFTH, we chose σ^{28} and σ^{38} as our research targets. The chimera of σ^{32} and σ^{28}, designated as σ^{32-28}, was designed by replacing the βFTH-interacting σ_4 segment of σ^{32} with the βFTH-interacting σ_4 segment of σ^{28}. The chimera of σ^{32} and σ^{38}, designated as σ^{32-38}, was designed by replacing the βFTH-interacting σ_4 region of σ^{32} with the βFTH-interacting σ_4 region of σ^{38} (Figure 3E). The calculated K_D values of WT, chimera σ^{32-28}, and chimera σ^{32-38} are 14.95 nM, 9.22 nM, 8.34 nM, respectively. Owing to the larger binding area, the binding affinity in this experiment is higher than that in Figure 2B, and σ^{32-28} and σ^{32-38} both enhanced the affinity of promoter DNA binding to the holoenzyme as shown by the result of the fluorescence polarization assay (Figure 3F). Similarly, both chimeras enhanced transcription activities (Figure 3G). These results indicate the

importance of σ_4–βFTH interaction in σ^{32}-promoter recognition, and also highlighted the important role of βFTH in orchestrating the recognition of other σ promoters. Collectively, our structural and biochemical results suggest that biased σ_4–βFTH configurations in different σs may be adopted to modulate binding affinity to promoters so as to orchestrate the recognition and regulation of different promoters.

4. Discussion

Bacterial cells sense and respond to different environmental conditions by regulating different expression regulons via activation of distinct σ-RNAP holoenzymes [53]. Certain RNAPs harboring group 1 and group 2 σ factors can transcribe the same promoter sets [54]. *E. coli* σ^{70} shares a high degree of protein sequence similarity with σ^{38} and prefers binding to similar DNA sequences at the -10 and -35 promoter elements [55]. In contrast, the protein sequences and target DNA sequence of other σ factors are less similar.

Our structure revealed that the recognition between σ^{32}-RPo and -35 element closely resembles that of σ^{24}-RPo [15] rather than that of σ^{28}-RPo [26], despite the fact that both σ^{32} and σ^{28} belong to group 3 (Figure 1E and Figure S4). By comparison, σ^{70}-RPo and σ^{38}-RPo strongly interact with -35 element and the spacer region, with both having six to eight residues participating in the interactions (Figure S4C,D,G,H), while σ^{24}-RPo interacts modestly with the -35 element and the spacer region, with four residues participating in the interactions (Figure S4A,E). It is worth noting that the interaction between σ^{28} and -35 element is the weakest (Figure S4B), consistent with the finding that β'ZBD is relocated to help strength the interaction with the -35 element [26]. Furthermore, our study revealed a relatively weak interaction between σ^{32} and $-35/-10$ spacer region mediated by T128 and K130 of σ^{32} (Figure 1G), which is in congruence with a previous study [48]. Collectively, these structural features are consistent with the fact that group 2 σs are more similar to housekeeping group 1 σs, and group 1 and group 2 σs account for the transcription of a majority of genes in bacteria [2].

Our structure may also help solve or explain some previous questions. Based on our structure, we speculate that phosphorylation of Y260 may inhibit σ^{32} activity [56] by attenuating the interaction between adjacent residues and the -35 element or by triggering an unpopular σ_4–βFTH configurations. Our structure also connects a series of disordered regions in σ^{32} previously reported in research on HSR: residues 47–55, termed feedback control region [57–59], are located in $\sigma_{2.1}$ and are partially protected by residues 57–66 of the clamp helix of β', which is the binding site for DnaKJ chaperones [60,61]. Sandwiched between $\sigma_{1.2}$ and $\sigma_{3.0}$, residues 122–144 (Region C) [62] and residues 263–284 (The C-terminal region) [63] are mainly responsible for binding with RNAP. In addition, as σ^{32} I54 (which was shown to play a crucial role in membrane-targeted instability of σ^{32} during HSR) [57] was fixed and protected by the helix of $\sigma_{2.2}$ and the clamp helix of the β' subunit, we speculate that cytoplasmic σ^{32} faces two mutually exclusive fates: either bind to RNAP to exert their active function or be inactivated through membrane localization.

From first engaging with promoter DNA to finally producing RNA, RNAP holoenzymes harboring promoters undergo several sequential conformational states, including promoter recognition (RPc), promoter melting (RPi), and bubble formation (RPo) [64]. Promoter melting is nucleated by the wedge residue, as shown in our study and in previous reports [15,65]. The hallmark of RPo maturation is the formation of an approximately 12-nt "bubble" around the promoter -10 element, which allows initial RNA synthesis and NTPs incorporation. W-dyad was found to wedge the transcription bubble in σ^{70}. While the presence of W-dyad is common in group 1 σ factors [66,67], residues harboring bulky hydrophobic sidechains are favored at corresponding sites in other σ factors [67]. Given the robust DNA-melting capacity of group 1 σ factors, it was believed that the W-dyad would be optimal for supporting the upstream transcription bubble. Our structure shows that H107 in σ^{32} replaces W433 in the W-dyad in σ^{70} to wedge the upstream transcription bubble, while W108 in σ^{32} resembles W434 in the W-dyad of σ^{70}. Our data also show that different σ factors employ distinct wedge residues in initiating transcription with the

following activity ranking: WW > HW > QR. This result is consistent with the result of the stopped-flow assay. Our result is in congruence with previous hypothesis that the W-dyad is the optimal choice for wedging the upstream ds/ss junction of the transcription bubble [65], giving its powerful DNA-melting capacity. Other residues such as H, N, and Q (Figure 1F and Figure S4I–J) with inferior promoter melting abilities may allow alternative σ factors to form RPo at a slower rate (Figure 2C,D), fine-tuning their specificity [15]. Variations in the residues at this very position may lead to differences in DNA-melting capabilities of different σ factors, leading to differential transcription activity and gene regulation [68].

During transcription initiation, conserved σ_4 contacts the βFTH and mediates recognition of the promoter -35 element [69]. Previous reports established that variations in spacer lengths greatly affects transcription activity and leads to the concurrent rotation of the σ_4–βFTH module, which plays a significant role in promoter recognition [70–72]. However, whether the σ_4–βFTH modules of different σs can allosterically affect promoter recognition has not been explored. Here, two chimeric σ factors ($\sigma^{32–28}$ and $\sigma^{32–38}$) with partial σ_4 domain replaced were designed to test the impact on DNA binding affinity and transcription activity, and it was surprising to find variation in DNA binding affinity and enhanced transcription activity with the chimeric proteins (Figure 3F,G). These results indicated the importance of σ_4–βFTH interaction in σ^{32}-promoter recognition and also highlighted the important role of βFTH in orchestrating the recognition of other σ promoters. Although our study shows that the σ_4–βFTH interaction affects transcription activity by influencing the binding affinity of σ_4 to the promoter, it seems that other steps such as promoter escape and transcription pausing may also play a role [16,49]. Nevertheless, our study indicates that the σ_4–βFTH interaction is tuned to balance the distinct transcription efficiencies of different σ factors.

In summary, our structure and supporting biochemical data identified a different promoter recognition and promoter melting mode for transcription initiation, including (1) a relatively weak interaction between σ^{32} and $-35/-10$ spacer that may account for less efficient promoter recognition [2]; (2) a histidine with inferior promoter melting ability that may allow σ^{32} to form RPo at a slower rate, fine-tuning its specificity; (3) a biased σ_4–βFTH configuration to modulate the affinity of binding to the promoter so as to orchestrate the recognition and regulation of different promoters. Our work will deepen our understanding of transcription initiation mechanisms of different σ^{32} factors as well as the biological function of σ^{32}.

Author Contributions: S.W. and L.M. conceived and supervised the project. Q.L. and F.W. prepared samples. J.W. performed cryo-EM data acquisition, data processing and model building. Q.L., T.C. and W.Y. conducted the fluorescence polarization assay and the stopped-flow assay. S.W., L.M. and Q.L. conducted structure data analysis and wrote the manuscript. All authors have read and agreed to the published version of the manuscript.

Institutional Review Board Statement: Not applicable.

Informed Consent Statement: Not applicable.

Data Availability Statement: Structure coordinates and cryo-EM density map of σ³²-RPo have been deposited in the Protein Data Bank and Electron Microscopy Data Bank under accession numbers 8HKC and EMD-34849, respectively.

Conflicts of Interest: The authors declare that they have no known competing financial interest or personal relationships that could have appeared to influence the work reported in this paper.

References

1. Ruff, E.F.; Record, J.M.T.; Artsimovitch, I. Initial Events in Bacterial Transcription Initiation. *Biomolecules* **2015**, *5*, 1035–1062. [CrossRef] [PubMed]
2. Feklistov, A.; Sharon, B.D.; Darst, S.A.; Gross, C.A. Bacterial sigma factors: A historical, structural, and genomic perspective. *Annu. Rev. Microbiol.* **2014**, *68*, 357–376. [CrossRef] [PubMed]
3. Chen, J.; Boyaci, H.; Campbell, E.A. Diverse and unified mechanisms of transcription initiation in bacteria. *Nat. Rev. Genet.* **2021**, *19*, 95–109. [CrossRef] [PubMed]
4. Gruber, T.M.; Gross, C.A. Multiple Sigma Subunits and the Partitioning of Bacterial Transcription Space. *Annu. Rev. Microbiol.* **2003**, *57*, 441–466. [CrossRef]
5. Shingler, V. Signal sensory systems that impact σ⁵⁴ -dependent transcription. *FEMS Microbiol. Rev.* **2011**, *35*, 425–440. [CrossRef] [PubMed]
6. Zhang, N.; Jovanovic, G.; McDonald, C.; Ces, O.; Zhang, X.; Buck, M. Transcription Regulation and Membrane Stress Management in Enterobacterial Pathogens. *Biophys. Infect.* **2016**, *915*, 207–230.
7. Pletnev, P.; Pupov, D.; Pshanichnaya, L.; Esyunina, D.; Petushkov, I.; Nesterchuk, M.; Osterman, I.; Rubtsova, M.; Mardanov, A.; Ravin, N.; et al. Rewiring of growth-dependent transcription regulation by a point mutation in region 1.1 of the housekeeping sigma factor. *Nucleic Acids Res.* **2020**, *48*, 10802–10819. [CrossRef] [PubMed]
8. Bae, B.; Davis, E.; Brown, D.; Campbell, E.A.; Wigneshwararaj, S.; Darst, S.A. Phage T7 Gp2 inhibition of *Escherichia coli* RNA polymerase involves misappropriation of sigma70 domain 1.1. *Proc. Natl. Acad. Sci. USA* **2013**, *110*, 19772–19777. [CrossRef]
9. Vuthoori, S.; Bowers, C.W.; McCracken, A.; Dombroski, A.J.; Hinton, D.M. Domain 1.1 of the sigma(70) subunit of *Escherichia coli* RNA polymerase modulates the formation of stable polymerase/promoter complexes. *J. Mol. Biol.* **2001**, *309*, 561–572. [CrossRef]
10. Zenkin, N.; Kulbachinskiy, A.; Yuzenkova, Y.; Mustaev, A.; Bass, I.; Severinov, K.; Brodolin, K. Region 1.2 of the RNA polymerase sigma subunit controls recognition of the -10 promoter element. *EMBO J.* **2007**, *26*, 955–964. [CrossRef]
11. Narayanan, A.; Vago, F.S.; Li, K.; Qayyum, M.Z.; Yernool, D.; Jiang, W.; Murakami, K.S. Cryo-EM structure of *Escherichia coli* sigma(70) RNA polymerase and promoter DNA complex revealed a role of sigma non-conserved region during the open complex formation. *J. Biol. Chem.* **2018**, *293*, 7367–7375. [CrossRef]
12. Mitchell, J.E.; Zheng, D.; Busby, S.J.; Minchin, S.D. Identification and analysis of 'extended -10' promoters in *Escherichia coli*. *Nucleic Acids Res.* **2003**, *31*, 4689–4695. [CrossRef] [PubMed]
13. Kumar, A.; Malloch, R.A.; Fujita, N.; Smillie, D.A.; Ishihama, A.; Hayward, R.S. The Minus 35-Recognition Region of *Escherichia coli* Sigma 70 is Inessential for Initiation of Transcription at an "Extended Minus 10" Promoter. *J. Mol. Biol.* **1993**, *232*, 406–418. [CrossRef] [PubMed]
14. Oguienko, A.; Petushkov, I.; Pupov, D.; Esyunina, D.; Kulbachinskiy, A. Universal functions of the sigma finger in alternative sigma factors during transcription initiation by bacterial RNA polymerase. *RNA Biol.* **2021**, *18*, 2028–2037. [CrossRef] [PubMed]
15. Fang, C.; Li, L.; Shen, L.; Shi, J.; Wang, S.; Feng, Y.; Zhang, Y. Structures and mechanism of transcription initiation by bacterial ECF factors. *Nucleic Acids Res.* **2019**, *47*, 7094–7104. [CrossRef]
16. Petushkov, I.; Esyunina, D.; Mekler, V.; Severinov, K.; Pupov, D.; Kulbachinskiy, A. Interplay between σ region 3.2 and secondary channel factors during promoter escape by bacterial RNA polymerase. *Biochem. J.* **2017**, *474*, 4053–4064. [CrossRef]
17. Murakami, K.S.; Masuda, S.; Campbell, E.A.; Muzzin, O.; Darst, S.A. Structural Basis of Transcription Initiation: An RNA Polymerase Holoenzyme-DNA Complex. *Science* **2002**, *296*, 1285–1290. [CrossRef]
18. Yura, T. Regulation of the heat shock response in *Escherichia coli*: History and perspectives. *Genes Genet. Syst.* **2019**, *94*, 103–108. [CrossRef]
19. Nagai, H.; Yuzawa, H.; Kanemori, M.; Yura, T. A distinct segment of the sigma 32 polypeptide is involved in DnaK-mediated negative control of the heat shock response in *Escherichia coli*. *Proc. Natl. Acad. Sci. USA* **1994**, *91*, 10280–10284. [CrossRef]
20. Nagai, H.; Yuzawa, H.; Yura, T. Interplay of two cis-acting mRNA regions in translational control of sigma 32 synthesis during the heat shock response of *Escherichia coli*. *Proc. Natl. Acad. Sci. USA* **1991**, *88*, 10515–10519. [CrossRef]
21. Kamath-Loeb, A.S.; Gross, C.A. Translational regulation of sigma 32 synthesis: Requirement for an internal control element. *J. Bacteriol.* **1991**, *173*, 3904–3906. [CrossRef] [PubMed]
22. Guisbert, E.; Herman, C.; Lu, C.Z.; Gross, C.A. A chaperone network controls the heat shock response in *E. coli*. *Genes Dev.* **2004**, *18*, 2812–2821. [CrossRef] [PubMed]
23. Herman, C.; Thévenet, D.; D'Ari, R.; Bouloc, P. Degradation of sigma 32, the heat shock regulator in *Escherichia coli*, is governed by HflB. *Proc. Natl. Acad. Sci. USA* **1995**, *92*, 3516–3520. [CrossRef]
24. Murakami, K.S. X-ray crystal structure of *Escherichia coli* RNA polymerase sigma70 holoenzyme. *J. Biol. Chem.* **2013**, *288*, 9126–9134. [CrossRef] [PubMed]

25. Liu, B.; Zuo, Y.; Steitz, T.A. Structures of *E. coli* sigmaS-transcription initiation complexes provide new insights into polymerase mechanism. *Proc. Natl. Acad. Sci. USA* **2016**, *113*, 4051–4056. [CrossRef]

26. Shi, W.; Zhou, W.; Zhang, B.; Huang, S.; Jiang, Y.; Schammel, A.; Hu, Y.; Liu, B. Structural basis of bacterial σ -mediated transcription reveals roles of the RNA polymerase zinc-binding domain. *EMBO J.* **2020**, *39*, e104389. [CrossRef]

27. Danson, A.E.; Jovanovic, M.; Buck, M.; Zhang, X. Mechanisms of σ(54)-Dependent Transcription Initiation and Regulation. *J. Mol. Biol.* **2019**, *431*, 3960–3974. [CrossRef] [PubMed]

28. Glyde, R.; Ye, F.; Darbari, V.C.; Zhang, N.; Buck, M.; Zhang, X. Structures of RNA Polymerase Closed and Intermediate Complexes Reveal Mechanisms of DNA Opening and Transcription Initiation. *Mol. Cell* **2017**, *67*, 106–116.e4. [CrossRef]

29. Yang, Y.; Darbari, V.C.; Zhang, N.; Lu, D.; Glyde, R.; Wang, Y.P.; Winkelman, J.T.; Gourse, R.L.; Murakami, K.S.; Buck, M.; et al. TRANSCRIPTION. Structures of the RNA polymerase-σ54 reveal new and conserved regulatory strategies. *Science* **2015**, *349*, 882–885. [CrossRef]

30. Svetlov, V.; Artsimovitch, I. Purification of bacterial RNA polymerase: Tools and protocols. *Methods Mol. Biol.* **2015**, *1276*, 13–29. [PubMed]

31. Helmann, J.D.; Chamberlin, M.J. Structure and function of bacterial sigma factors. *Annu. Rev. Biochem.* **1988**, *57*, 839–872. [CrossRef] [PubMed]

32. Wang, F.; Shi, J.; He, D.; Tong, B.; Zhang, C.; Wen, A.; Zhang, Y.; Feng, Y.; Lin, W. Structural basis for transcription inhibition by *E. coli* SspA. *Nucleic Acids Res.* **2020**, *48*, 9931–9942. [CrossRef] [PubMed]

33. You, L.; Shi, J.; Shen, L.; Li, L.; Fang, C.; Yu, C.; Cheng, W.; Feng, Y.; Zhang, Y. Structural basis for transcription antitermination at bacterial intrinsic terminator. *Nat. Commun.* **2019**, *10*, 3048. [CrossRef] [PubMed]

34. Maziarz, M.; Garcia-Marcos, M. Fluorescence polarization assays to measure interactions between Gα subunits of heterotrimeric G proteins and regulatory motifs. In *Methods in Cell Biology*; Academic Press: New York, NY, USA, 2017; Volume 142, pp. 133–143.

35. KKo, J.; Heyduk, T. Kinetics of promoter escape by bacterial RNA polymerase: Effects of promoter contacts and transcription bubble collapse. *Biochem. J.* **2014**, *463*, 135–144. [CrossRef]

36. Mastronarde, D.N. Automated electron microscope tomography using robust prediction of specimen movements. *J. Struct. Biol.* **2005**, *152*, 36–51. [CrossRef] [PubMed]

37. Zheng, S.Q.; Palovcak, E.; Armache, J.-P.; Verba, K.A.; Cheng, Y.; Agard, D.A. MotionCor2: Anisotropic correction of beam-induced motion for improved cryo-electron microscopy. *Nat. Methods* **2017**, *14*, 331–332. [CrossRef] [PubMed]

38. Rohou, A.; Grigorieff, N. CTFFIND4: Fast and accurate defocus estimation from electron micrographs. *J. Struct. Biol.* **2015**, *192*, 216–221. [CrossRef]

39. Scheres, S.H. RELION: Implementation of a Bayesian approach to cryo-EM structure determination. *J. Struct. Biol.* **2012**, *180*, 519–530. [CrossRef]

40. Kang, J.Y.; Olinares, P.D.; Chen, J.; Campbell, E.A.; Mustaev, A.; Chait, B.T.; Gottesman, M.E.; Darst, S.A. Structural basis of transcription arrest by coliphage HK022 Nun in an *Escherichia coli* RNA polymerase elongation complex. *eLife* **2017**, *6*, e25478. [CrossRef]

41. Pettersen, E.F.; Goddard, T.D.; Huang, C.C.; Couch, G.S.; Greenblatt, D.M.; Meng, E.C.; Ferrin, T.E. UCSF Chimera? A visualization system for exploratory research and analysis. *J. Comput. Chem.* **2004**, *25*, 1605–1612. [CrossRef]

42. Emsley, P.; Cowtan, K. Coot: Model-building tools for molecular graphics. *Acta Crystallogr. D Biol. Crystallogr.* **2004**, *60*, 2126–2132. [CrossRef]

43. Adams, P.D.; Afonine, P.V.; Bunkóczi, G.; Chen, V.B.; Davis, I.W.; Echols, N.; Headd, J.J.; Hung, L.W.; Kapral, G.J.; Grosse-Kunstleve, R.W.; et al. PHENIX: A comprehensive Python-based system for macromolecular structure solution. *Acta Crystallogr. D Biol. Crystallogr.* **2010**, *66*, 213–221. [CrossRef]

44. Xu, J.; Cui, K.; Shen, L.; Shi, J.; Li, L.; You, L.; Fang, C.; Zhao, G.; Feng, Y.; Yang, B.; et al. Crl activates transcription by stabilizing active conformation of the master stress transcription initiation factor. *eLife* **2019**, *8*, e50928. [CrossRef]

45. Qayyum, M.Z.; Molodtsov, V.; Renda, A.; Murakami, K.S. Structural basis of RNA polymerase recycling by the Swi2/Snf2 family of ATPase RapA in *Escherichia coli*. *J. Biol. Chem.* **2021**, *297*, 101404. [CrossRef]

46. Vishwakarma, R.K.; Cao, A.M.; Morichaud, Z.; Perumal, A.S.; Margeat, E.; Brodolin, K. Single-molecule analysis reveals the mechanism of transcription activation in M. tuberculosis. *Sci. Adv.* **2018**, *4*, eaao5498. [CrossRef] [PubMed]

47. Schwartz, E.C.; Shekhtman, A.; Dutta, K.; Pratt, M.R.; Cowburn, D.; Darst, S.; Muir, T.W. A full-length group 1 bacterial sigma factor adopts a compact structure incompatible with DNA binding. *Chem. Biol.* **2008**, *15*, 1091–1103. [CrossRef] [PubMed]

48. Koo, B.M.; Rhodius, V.A.; Campbell, E.A.; Gross, C.A. Dissection of recognition determinants of *Escherichia coli* sigma32 suggests a composite -10 region with an 'extended -10' motif and a core -10 element. *Mol. Microbiol.* **2009**, *72*, 815–829. [CrossRef] [PubMed]

49. Brodolin, K.; Morichaud, Z. Region 4 of the RNA polymerase sigma subunit counteracts pausing during initial transcription. *J. Biol. Chem.* **2021**, *296*, 100253. [CrossRef]

50. Saecker, R.M.; Chen, J.; Chiu, C.E.; Malone, B.; Sotiris, J.; Ebrahim, M.; Yen, L.Y.; Eng, E.T.; Darst, S.A. Structural origins of *Escherichia coli* RNA polymerase open promoter complex stability. *Proc. Natl. Acad. Sci. USA* **2021**, *118*, e2112877118. [CrossRef]

51. Campagne, S.; Marsh, M.E.; Capitani, G.; Vorholt, J.A.; Allain, F.H. Structural basis for -10 promoter element melting by environmentally induced sigma factors. *Nat. Struct. Mol. Biol.* **2014**, *21*, 269–276. [CrossRef]

52. Rammohan, J.; Ruiz Manzano, A.; Garner, A.L.; Stallings, C.L.; Galburt, E.A. CarD stabilizes mycobacterial open complexes via a two-tiered kinetic mechanism. *Nucleic Acids Res.* **2015**, *43*, 3272–3285. [CrossRef] [PubMed]

53. Österberg, S.; del Peso-Santos, T.; Shingler, V. Regulation of alternative sigma factor use. *Annu. Rev. Microbiol.* **2011**, *65*, 37–55. [CrossRef] [PubMed]

54. Rodrigue, S.; Provvedi, R.; Jacques, P.E.; Gaudreau, L.; Manganelli, R. The sigma factors of Mycobacterium tuberculosis. *FEMS Microbiol. Rev.* **2006**, *30*, 926–941. [CrossRef]

55. Gaal, T.; Ross, W.; Estrem, S.T.; Nguyen, L.H.; Burgess, R.R.; Gourse, R.L. Promoter recognition and discrimination by EsigmaS RNA polymerase. *Mol. Microbiol.* **2001**, *42*, 939–954. [CrossRef] [PubMed]

56. Klein, G.; Dartigalongue, C.; Raina, S. Phosphorylation-mediated regulation of heat shock response in *Escherichia coli*. *Mol. Microbiol.* **2003**, *48*, 269–285. [CrossRef]

57. Lim, B.; Miyazaki, R.; Neher, S.; Siegele, D.A.; Ito, K.; Walter, P.; Akiyama, Y.; Yura, T.; Gross, C.A. Heat shock transcription factor σ32 co-opts the signal recognition particle to regulate protein homeostasis in *E. coli*. *PLoS Biol.* **2013**, *11*, e1001735. [CrossRef]

58. Yura, T.; Guisbert, E.; Poritz, M.; Lu, C.Z.; Campbell, E.; Gross, C.A. Analysis of sigma32 mutants defective in chaperone-mediated feedback control reveals unexpected complexity of the heat shock response. *Proc. Natl. Acad. Sci. USA* **2007**, *104*, 17638–17643. [CrossRef]

59. Horikoshi, M.; Yura, T.; Tsuchimoto, S.; Fukumori, Y.; Kanemori, M. Conserved region 2.1 of *Escherichia coli* heat shock transcription factor sigma32 is required for modulating both metabolic stability and transcriptional activity. *J. Bacteriol.* **2004**, *186*, 7474–7480. [CrossRef]

60. Suzuki, H.; Ikeda, A.; Tsuchimoto, S.; Adachi, K.; Noguchi, A.; Fukumori, Y.; Kanemori, M. Synergistic binding of DnaJ and DnaK chaperones to heat shock transcription factor σ32 ensures its characteristic high metabolic instability: Implications for heat shock protein 70 (Hsp70)-Hsp40 mode of function. *J. Biol. Chem.* **2012**, *287*, 19275–19283. [CrossRef]

61. Rodriguez, F.; Arsène-Ploetze, F.; Rist, W.; Rüdiger, S.; Schneider-Mergener, J.; Mayer, M.; Bukau, B. Molecular basis for regulation of the heat shock transcription factor sigma32 by the DnaK and DnaJ chaperones. *Molecular Cell* **2008**, *32*, 347–358. [CrossRef]

62. Arsene, F.; Tomoyasu, T.; Mogk, A.; Schirra, C.; Schulze-Specking, A.; Bukau, B. Role of region C in regulation of the heat shock gene-specific sigma factor of *Escherichia coli*, sigma32. *J. Bacteriol.* **1999**, *181*, 3552–3561. [CrossRef] [PubMed]

63. Tomoyasu, T.; Arsene, F.; Ogura, T.; Bukau, B. The C terminus of sigma(32) is not essential for degradation by FtsH. *J. Bacteriol.* **2001**, *183*, 5911–5917. [CrossRef] [PubMed]

64. Chen, J.; Chiu, C.; Gopalkrishnan, S.; Chen, A.Y.; Olinares PD, B.; Saecker, R.M.; Winkelman, J.T.; Maloney, M.F.; Chait, B.T.; Ross, W.; et al. Stepwise Promoter Melting by Bacterial RNA Polymerase. *Mol. Cell* **2020**, *78*, 275–288.e276. [CrossRef] [PubMed]

65. Bae, B.; Feklistov, A.; Lass-Napiorkowska, A.; Landick, R.; Darst, S.A. Structure of a bacterial RNA polymerase holoenzyme open promoter complex. *eLife* **2015**, *4*, e08504. [CrossRef]

66. Gruber, T.M.; Bryant, D.A. Molecular systematic studies of eubacteria, using sigma70-type sigma factors of group 1 and group 2. *J. Bacteriol.* **1997**, *179*, 1734–1747. [CrossRef]

67. Lonetto, M.; Gribskov, M.; Gross, C.A. The sigma 70 family: Sequence conservation and evolutionary relationships. *J. Bacteriol.* **1992**, *174*, 3843–3849. [CrossRef]

68. Koo, B.M.; Rhodius, V.A.; Nonaka, G.; deHaseth, P.L.; Gross, C.A. Reduced capacity of alternative sigmas to melt promoters ensures stringent promoter recognition. *Genes Dev.* **2009**, *23*, 2426–2436. [CrossRef]

69. Geszvain, K.; Gruber, T.M.; Mooney, R.A.; Gross, C.A.; Landick, R. A hydrophobic patch on the flap-tip helix of *E. coli* RNA polymerase mediates sigma(70) region 4 function. *J. Mol. Biol.* **2004**, *343*, 569–587. [CrossRef]

70. Fang, C.; Philips, S.J.; Wu, X.; Chen, K.; Shi, J.; Shen, L.; Xu, J.; Feng, Y.; O'Halloran, T.V.; Zhang, Y. CueR activates transcription through a DNA distortion mechanism. *Nat. Chem. Biol.* **2021**, *17*, 57–64. [CrossRef]

71. Fang, C.; Li, L.; Zhao, Y.; Wu, X.; Philips, S.; You, L.; Zhong, M.; Shi, X.; O'Halloran, T.; Li, Q.; et al. The bacterial multidrug resistance regulator BmrR distorts promoter DNA to activate transcription. *Nat. Commun.* **2020**, *11*, 6284. [CrossRef]

72. Zuo, Y.; Steitz, T.A. Crystal structures of the *E. coli* transcription initiation complexes with a complete bubble. *Mol. Cell* **2015**, *58*, 534–540. [CrossRef] [PubMed]